REPORT DOCUMENTATION PAGE

AFRL-SR-BL-TR-00-

0627

88

1. AGENCY USE ONLY *(Leave blank)*	2. REPORT DATE	3. REPORT TYPE AND DATES COVERED
	03 Nov 00	Final Report 01 Jan 98 To 31 Mar 00

4. TITLE AND SUBTITLE
A Robust Scheme for Control of Skin Friction and Heat Transfer in Turbulent Boundary Layers VIA a New Instability Mechanism

5. FUNDING NUMBERS
F49620-98-1-0150

6. AUTHOR(S)
Fazle Hussain

7. PERFORMING ORGANIZATION NAME(S) AND ADDRESS(ES)
Department of Mechanical Engineering
University of Houston
Houston TX 77204-4792

8. PERFORMING ORGANIZATION REPORT NUMBER

9. SPONSORING/MONITORING AGENCY NAME(S) AND ADDRESS(ES)
AFOSR/NA
801 N. Randolph St.
Arlington VA 22203

10. SPONSORING/MONITORING AGENCY REPORT NUMBER

11. SUPPLEMENTARY NOTES

12a. DISTRIBUTION AVAILABILITY STATEMENT
Aproved for public release; distribution is unlimited

12b. DISTRIBUTION CODE

13. ABSTRACT *(Maximum 200 words)*

Using direct numerical simulations of turbulent channel flow, we present new insight into the generation of streamwise vortices near the wall, aud an associated drag reduction strategy. Growth of x-dependent spanwise velocity disturbances w(x) is shown to occur via two mechanisms: (i) linear transient growth, which dominates early-time evolution, and (ii) linear normal-mode instability, dominant asymptotically at late time (for frozen base flow streaks). Approximately 25% of streaks extracted from near-wall turbulence are shown to be strong enough for linear instability (above a critical vortex line Lift angle). However, due to viscous annihilation of streak normal vorticity COy, normal mode growth ceases after a factor of two energy growth. In contrast, the linear transient disturbance produces a 20-fold amplification, due to its rapid, early-time growth before significant viscous streak decay. Thus, linear transient growth of w(x) is revealed as a new, apparently dominant, generation mechanism of x-dependent turbulent energy near the wall.

14. SUBJECT TERMS
A Robust Scheme for Control of Skin Friction and Heat Transfer in Turbulent Boundary Layers via a New Instability Mechanism

15. NUMBER OF PAGES

16. PRICE CODE

17. SECURITY CLASSIFICATION OF REPORT	18. SECURITY CLASSIFICATION OF THIS PAGE	19. SECURITY CLASSIFICATION OF ABSTRACT	20. LIMITATION OF ABSTRACT
Unclassified	Unclassified	Unclassified	UL

FINAL REPORT: A Robust Scheme for Control of Skin Friction and Heat Transfer in Turbulent Boundary Layers via a New Instability Mechanism

AFOSR GRANT NUMBER F49620-98-1-0150

Fazle Hussain
Department of Mechanical Engineering
University of Houston, Houston Texas 77204-4792

Research performed under this grant comprised two aspects, namely: (i) direct numerical simulations to understand the instability mechanism generating drag-enhancing near-wall vortices, and (ii) experiments to develop drag control techniques aiming to suppress the drag-enhancing vortices. These two aspects of our research are separately described below.

I. Direct Numerical Simulations

Summary. Using direct numerical simulations of turbulent channel flow, we present new insight into the generation of streamwise vortices near the wall, and an associated drag reduction strategy. Growth of x-dependent spanwise velocity disturbances $w(x)$ is shown to occur via two mechanisms: (i) linear transient growth, which dominates early-time evolution, and (ii) linear normal-mode instability, dominant asymptotically at late time (for frozen base flow streaks). Approximately 25% of streaks extracted from near-wall turbulence are shown to be strong enough for linear instability (above a critical vortex line lift angle). However, due to viscous annihilation of streak normal vorticity ω_y, normal mode growth ceases after a factor of two energy growth. In contrast, the linear transient disturbance produces a 20-fold amplification, due to its rapid, early-time growth before significant viscous streak decay. Thus, linear transient growth of $w(x)$ is revealed as a new, apparently dominant, generation mechanism of x-dependent turbulent energy near the wall.

Combined transient growth/instability of lifted, vortex-free low-speed streaks (above the instability cutoff of streak strength) is shown to generate new streamwise vortices, which dominate near-wall turbulence phenomena. This new vortex formation mechanism consists of: (i) streak waviness in the horizontal plane caused by $w(x)$ disturbance growth, (ii) generation of horizontal sheets of streamwise vorticity and induction of positive stretching $\partial u/\partial x$ (*i.e.* positive VISA), inherent to streak waviness, and finally (iii) vorticity sheet collapse via stretching (rather than roll-up) into streamwise vortices. Significantly, the 3D features of the (instantaneous) vortices generated by transient/instability growth agree well with the coherent structures educed (*i.e.* ensemble-averaged) from fully turbulent flow, suggesting the prevalence of this mechanism. Results suggest promising new strategies for drag and heat transfer control, involving large-scale (hence more durable) actuators, without requiring wall sensors or control logic.

1. Introduction

There is an evolving consensus that the increased drag and heat transfer in turbulent boundary layers are due to near-wall vortical *coherent structures* (CS). Viable control of near-wall turbulence, as yet largely unrealized in practice, has the potential for enormous savings in fuel costs via drag reduction for aircraft, marine transport vehicles, pipelines, and heat transfer management for high-temperature gas turbines. Although a barrage of drag reduction strategies have been studied extensively – *e.g.* compliant walls, polymer additives, riblets, microbubbles, electromagnetic forces, active walls with MEMS, among many others – their engineering application has remained scarce. A lack of successful implementation of boundary layer control can generally be traced to two key difficulties: (i) tiny spatial scales of near-wall streamwise CS (~0.1 mm) and (ii) incomplete understanding of the dynamics of CS initiation and evolution.

To address these inherent obstacles, we propose here new control approaches which explicitly utilize recent advances in the understanding of near-wall turbulence physics. The prominence of streamwise vortical coherent structures (CS) in near-wall turbulence is now well accepted (*e.g.* see Robinson 1991), as is their critical role in the elevated drag in turbulent boundary layers. The transport enhancing effect of near-wall CS is well understood. These CS sweep near-wall fluid toward the wall on one CS flank and eject it away from the wall on the other. Drag and heat transfer are enhanced by the wallward motion, which steepens the wall gradients of streamwise velocity U. Note that the gradient reduction on the outward motion side of vortices is relatively smaller, resulting in enhancement of mean wallward momentum transfer due to near-wall vortices.

The most logical approach to CS-based reduction of drag and heat transfer is to simply prevent vortex regeneration in the first place (in contrast to many approaches which counteract the wall interaction of fully developed CS). Although it has long been hypothesized that a major source of turbulence production near the wall is the instability of inflectional low-speed streaks (*e.g.* Kline *et al.* 1967; Swearingen & Blackwelder 1987; Hamilton *et al.* 1995), the issue remains unresolved. In particular, it is currently unknown whether streaks of sufficient strength for instability actually occur in fully-developed near-wall turbulence. Additionally, the influence on streak instability growth of viscous annihilation of streak normal vorticity is yet to be quantified, as is the possibility of linear transient growth. Finally, the relationship between streak disturbance growth and the formation mechanism of longitudinal vortices is poorly understood, which has prevented the development of streak disturbance control strategies aimed at drag reduction.

To date, we have demonstrated (Schoppa & Hussain 1997) that the CS (Jeong & Hussain 1992; Jeong *et al.* 1997) extracted from fully developed near-wall turbulence can be directly created by 3D inviscid instability of lifted streaks near a single wall (created by previous "parent" vortices, no longer present), the generation mechanism being akin to that of streamwise vortices in free shear layers by oblique mode instability (Schoppa *et al.* 1995). This new-found association of near-wall CS formation with instability mechanisms opens up promising avenues for explaining and especially controlling near-wall turbulence, noting the documented success of experimental instability control in both free- and wall-bounded shear flows (*e.g.* see Hussain 1986).

To suppress CS via control of streak disturbance growth (responsible for CS formation), there are two possibilities: either (i) counteract existing perturbations which would otherwise generate new CS, or (ii) stabilize the base flow streaks. Pursuit of (i) would necessitate instantaneous and small-scale detection and control, which would suffer from the durability problems faced by microscale active wall elements. Approach (ii) is very attractive from the standpoint of large-scale (hence more robust) control,

wherein numerous (perhaps thousands of) streaks may be stabilized together – hence suppressing new CS formation over an extended spatial domain – with a single robust actuator, involving time-independent control and no flow sensing.

The primary objective of this paper is to summarize our latest findings regarding streak disturbance growth and vortex generation. We demonstrate the underlying mechanism of CS formation, driven by nonlinear evolution of 3D disturbances of lifted low-speed streaks, distinguishing between linear (normal-mode) instability and linear transient growth.

2. Computational Approach

In the following, we address streak instability-induced vortex generation and its control using direct numerical simulations of the Navier-Stokes equations. Periodic boundary conditions are used in x and z, and the no-slip condition is applied on the two walls normal to y; see Kim *et al.* (1987) for the simulation algorithm details. The spatial discretization and Re are chosen so that all dynamically significant lengthscales are resolved (*i.e.* a finer computational grid does not markedly affect the solution); thus, no subgrid-scale turbulence model is necessary. Code validation and accuracy checks were performed by comparing the growth rates for simulated 2D and 3D (oblique) Orr-Sommerfeld modes of the laminar (parabolic profile) flow with independent stability analysis results (agreeing within 1%).

To better isolate instability and the subsequent vortex formation, we use the minimum outer Reynolds number $Re=U_c h/\nu=2000$ (U_c is the centerline velocity of the $2h$ wide channel for a laminar flow with the same volume flowrate) and the minimum domain sizes in x and z for sustained channel flow turbulence – the so-called "minimal flow unit" of Jimenez & Moin (1991). For simulations of isolated vortex regeneration, a constant volume flux is maintained, and 32x129x32 grid points are used in x, y, and z respectively.

3. Disturbance growth of near-wall streaks

The two most prominent structural features of near-wall turbulence are illustrated in Fig. 1: (i) "streaks" of low momentum fluid which has been lifted into the buffer region, and (ii) elongated longitudinal vortices, illustrated by the Jeong & Hussain (1995) vortex definition. It is now well-accepted that the streaks are generated by the lifting of low-speed fluid near the wall by the normal velocity induced by streamwise vortices; this is consistent with the close proximity of streaks to streamwise vortices in Fig. 1. Note also that many regions of streaks are devoid of nearby streamwise vortices, indicating that the characteristic elongation of streaks is due to the advection of streamwise vortices, which leave lifted low-speed fluid underneath them in their wake. Here, we reveal a more subtle and dynamically significant role of streaks, as a breeding ground for new streamwise CS via streak instability.

3.1 Linear instability

To evaluate the role of streak instability in vortex generation, we first consider three-dimensional disturbances of a class of two-dimensional base flows, representing the range of low-speed streak strengths (*i.e.* magnitude of ω_y^+ flanking streak, defined later as θ_{20}) observed in fully-developed near-wall turbulence. Our focus here is on "lifted" streaks, which are detectable even outside the buffer layer (*e.g.* at $y^+=30$; see Robinson

1991). Note the distinction of these lifted streaks from more numerous sublayer streaks, which are localized to the viscous sublayer but do not extend into the buffer layer. [Of course, a lifted streak is typically traceable to a particular sublayer streak, but the inverse is not generally true.] We illustrate the unique, inherently three-dimensional mechanism of (inviscid) instability using vortex dynamics concepts, and reveal significant base flow modification due to viscous cross-diffusion of streak (wall-normal) vorticity.

To isolate the three-dimensional dynamics of lifted streaks, in a "clean" environment free from existing structures and incoherent turbulence (including perturbations presumably induced by larger-scale outer vortices), we analyze a z-periodic row of parallel (x-independent) low-speed streaks, initially containing no vortices or ω_x whatsoever (*i.e.* $U(y,z)$ only). Additionally, the streaks are localized to a single wall, to prevent the second wall (far removed in z) from strongly influencing the essential near-wall dynamics, such influence being minimal in channel and plane Couette flows at sufficiently high *Re*. Note that this class of base flows is inviscidly steady (for a constant volume flux) as required for stability analysis, and is qualitatively consistent with near-wall streaks observed both in minimal (*e.g.* see Jimenez & Moin 1991; Schoppa & Hussain 1997) and full-domain (*e.g.* see Robinson 1991) turbulent flow, the latter showing regions along individual streaks to be commonly devoid of nearby streamwise vortices.

As a representation of vortex-free, lifted low-speed streaks of variable strength, we consider a base flow family of the form

$$U(y,z)=U_0(y)+(\Delta u/2)\cos(\beta_s z)\, g(y)$$
$$V=W=0\,, \qquad (1)$$

where $U_0(y)$ is the turbulent mean velocity profile and $g(y)$ is an amplitude function which satisfies the no-slip condition at $y=0$ and localizes the streaks' velocity defect to a single near-wall region (*i.e.* $y^+<60$). A function satisfying these requirements is $g(y)\sim y\cdot\exp(-\sigma y^2)$, normalized to unity and with σ specified such that the maximum streak vorticity $\omega_y|_{max}=\beta_s\Delta u/2$ and normal circulation per unit length Δu occur in the range $y^+=20$-30, consistent with lifted streaks.

As illustrated in Fig. 2b for a moderately strong streak (circulation specified with Δu in (1)), the base flow (1) closely resembles lifted low speed streaks prominent both in minimal channel turbulence (Fig. 2a) and in virtually any (y,z) cross-section of full-domain turbulence (*e.g.* see Kim *et al.* 1987). In accordance with (1), all streak base flows considered here are even-symmetric about $z=0$, *i.e.* $U(y,z)=U(y,-z)$. Note that the streaks are localized to a single wall (via $g(y)$ in (1)), and hence are essentially decoupled from the second wall. Compared to single-walled streaks, the influence of a second no-slip wall immediately above the streak is twofold: (i) additional y symmetry is imposed on the linear eigenmodes and (ii) the subsequent nonlinear evolution is fundamentally altered (Schoppa & Hussain 1998a).

For illustrative purposes, it is useful to represent the "strength" of lifted streaks in terms of the maximum inclination angle θ of vortex lines on the streak flank, given locally by $\theta=\tan^{-1}(|\omega_y|/|\omega_z|)$. In this way, the strength of the base flow streaks (1) may be characterized conveniently as the maximum vortex line lift angle, *e.g.* defined at $y^+=20$ as $\theta_{20}=\tan^{-1}[\omega_y|_{max}/(dU_0/dy(y^+=20))]$ with $\omega_y|_{max}=\beta_s\Delta u/2$. Note that this provides a visual representation of the relative magnitude of the spanwise shear $\partial u/\partial z \approx \omega_y$ on the streak flank. For example, for the moderately strong streak in Fig. 2b, the inclination angle of

streak vortex lines at the z-location of $\omega_y|_{max}$ at $y^+=20$ (equivalent to U contours for x-independent flow) is $\theta_{20}=56°$.

Note that the amplitude function $g(y)$ in (1) determines the strength of the local curved shear layer (*e.g.* local maxima of $\partial U/\partial y(y,\beta_s z=\pi)$) residing on the crest of the lifted streak. Instability growth rates for sinuous modes (defined below) – the focus of this study – are found to be relatively insensitive to the strength of this shear layer and hence to the amplitude function $g(y)$. Note, however, that the typically slower-growing varicose instability mode is found to depend crucially on the vorticity magnitude of this wall-detached shear layer. Thus, varicose modes, found to be stable here, may indeed be unstable for artificially strong streak-top shear, although the growth rate is significantly smaller than for the sinuous modes (Yu & Liu 1991).

For all flows considered here, the streak spanwise wavenumber β_s in (1) is chosen as $2\pi/\beta_s^+=100$, corresponding to a 100 wall unit spanwise spacing of adjacent low-speed streaks. Although results below may subsequently be applied to address the predominance of this particular streak spacing, our focus here is on vortex generation from developed streaks, whose spacing must thus be specified *a priori*. Note that the complementary mechanism of streak formation, *i.e.* lift-up of low-speed fluid near the wall by the induced v of (mature) streamwise vortices, is easily understood and now well-accepted.

In accordance with Floquet theory for the z-periodic base flows represented in (1), we consider temporal disturbances (denoted by primes) of the form

$$\begin{pmatrix} u' \\ v' \\ w' \\ p' \end{pmatrix}(x,y,z,t) = \Re\left[\begin{pmatrix} \tilde{u} \\ \tilde{v} \\ \tilde{w} \\ \tilde{p} \end{pmatrix}(y,z)\, e^{i(\alpha x+\beta z)} e^{\sigma t}\right], \qquad (2)$$

where the streamwise α and spanwise wavenumber β are real, and the eigenvalues σ are generally complex. The tilded complex eigenfunctions are periodic in z with the streak spanwise wavenumber β_s, and the velocity eigenfunctions vanish at the upper and lower walls (y=0,2h).

To quantify possible linear instability of streaks characteristic of fully-developed near-wall turbulence, we first discuss three-dimensional solutions of the stability equations for the class of streaks represented by the base flow (1). Realizable characteristics of streaks in near-wall turbulence are then obtained via a streak eduction procedure, permitting a statistical evaluation of these streaks' degree of instability.

Due to the finite-amplitude two-dimensionality of the base flow (1), direct solution of the associated two-dimensional p.d.e. eigenvalue problem necessitates a complex computational algorithm such as spectral collocation, involving eigensolution of large, non-sparse matrices. This poses a formidable computational challenge for the single-walled streaks addressed here, where the gap between walls is much larger than the near-wall region to be resolved. As an alternative (frequently used), we analyze the instability of the streak flow (1) using direct numerical simulations of the Navier-Stokes equations, initialized with effectively infinitesimal disturbances. This approach is well-suited for extracting highly resolved most-unstable (or least-stable) modes, and is used here for finite *Re* stability analysis via "freezing" of the x-independent modes representing the base flow in DNS. Additionally, individual modes of interest may be isolated through appropriate choices of small-amplitude disturbances, including specification of the

streamwise and spanwise wavenumbers (α,β) and either a varicose or sinuous spanwise symmetry. For example, to excite only the z-fundamental (*i.e.* β=0), sinuous mode of streak instability, we initialize (1) along with an x-dependent spanwise velocity perturbation of the form

$$w(x,y)=\varepsilon \sin(\alpha x) y \exp(-\sigma y^2), \qquad (3)$$

where ε is the (linear) disturbance amplitude and σ is a normal decay parameter which localizes the perturbation to the near-wall region (y^+<60). Provided that an arbitrary perturbation such as (3) has a non-zero projection onto the instability mode of interest, the disturbance will naturally evolve to this eigenmode. Lock-on of the simulation to a given instability mode is signaled by sustained exponential growth of $E_{1n}(t)$ (with $n\neq0$), the volume-integrated energy in all Fourier modes with an x-wavenumber of α.

As indicated in Fig. 3, a moderately strong streak with $\omega_y^+|_{max}$=0.35 (streak lift angle θ_{20}=56°) and $2\pi/\beta_s^+$=100 (Fig. 2b) is indeed linearly unstable, with a maximum growth rate of approximately σ^+=0.012 (*i.e.* doubling of three-dimensional energy in 29 wall time units). Interestingly, the maximal growth rate occurs for a streamwise wavelength of approximately 300 wall units, closely corresponding to the minimum x-wavelength required for turbulence sustenance (Jimenez & Moin 1991) at Re=2000 (L_x^+=290). Note that the 400 wall unit streamwise extent of a symmetric pair of educed near-wall coherent structures (Jeong *et al.* 1997) also exhibits a nearly maximal streak instability growth rate. Collectively, these results indicate that the characteristic streamwise wavelength of near-wall structures (300-400 wall units) is consistent with a predominant streak instability mechanism. As a further note, the minimal x-wavelength for sustained turbulent plane Couette flow (Hamilton *et al.* 1995) – approximately 170 wall units – differs significantly from that of minimal channel flow (Fig. 3). This discrepancy reflects other fundamental differences in the underlying instability mechanisms of minimal channel and Couette turbulence (see Schoppa & Hussain 1998a for details).

Having shown linear instability of a $U(y,z)$ distribution visually representative of instantaneous lifted streaks in near-wall turbulence, we now quantify the growth rate variation with streak strength, defined in terms of the lift angle θ_{20} (defined above). Note that for a fixed streak spacing, θ_{20} determines the height as well as flank-slope of lifted U contours (Fig. 2b). Significantly, sinuous streak instability requires a threshold streak lift angle θ_{20} of approximately 50° (corresponding to a streak vorticity of $\omega_y|_{max}$=0.27), reflected by the region of positive growth rate σ in Fig. 4. Thus, lifted streaks may be either passive (stable) or dynamically active (unstable) to small-amplitude sinuous perturbations, depending upon rather slight (*i.e.* virtually indistinguishable visually) differences in streak vorticity. For instance, streaks with small difference in streak angle – say 45° (stable) and 55° (unstable with significant growth rate) – cannot be easily distinguished. Furthermore, this instability threshold indicates that well-defined lifted streaks, even those extending past the buffer layer, are not necessarily unstable. Past the instability cutoff, the growth rate increases approximately linearly with the streak vorticity $\omega_y|_{max}$ (nearly linearly with θ_{20} for this angle range), suggesting a dominant influence of $U(z)$ shear in driving sinuous instability (see also Yu & Liu 1991 for Gortler streaks). Nevertheless, as shown below, the sinuous mode is inherently three-dimensional, and its growth mechanism is distinct from that of a one-dimensional $U(z)$ wake profile. Based on the instability cutoff behavior in Fig. 4 (consistent also with the

stability of the turbulent mean profile $U(y)$ for channel flow), the straightening of streak vortex lines by background ω_z is a strongly stabilizing effect for sinuous streak instability.

Owing to the threshold behavior in Fig. 4, the role of (linear) streak instability in fully developed near-wall turbulence relies critically on the magnitudes of streak $\partial u/\partial z$ (hence streak lift angle) actually realized. To obtain conditional streak statistics, an eduction procedure is used to extract individual streak realizations from fully developed turbulent channel flow at Re=1800 (Kim *et al.* 1987 database). To obtain local, unsmeared vorticity statistics isolated to streaks, the following streak eduction procedure is defined:

(i) Regions of $u'<0$ are identified in a specified y plane (black regions in Fig. 1).
(ii) Within each $u'<0$ region, the (x_c,z_c) locations of local minima of u' are identified as streak centers.
(iii) The first local maxima of $|\partial u/\partial z|$ in z is identified on either side of each streak center (x_c,z_c). The larger of these two $|\partial u/\partial z|$ values is recorded as the maximum vorticity for each streak realization.

For 50 time realizations of full-domain turbulence (L_x^+~1400; L_z^+~450), spanning 500 wall time units, this eduction procedure performed at y^+=20 extracts approximately 11,300 streak (y,z) cross-sections. Dividing the z domain size by the average number of realizations per unit x (for an x grid spacing of Δx^+=29), an average spanwise spacing of 96 wall units is obtained between accepted realizations. The close agreement of this educed streak count with the well-accepted z-spacing of streaks (~100 wall units) confirms that streaks are adequately captured and that false triggers or omissions are negligible.

Subject to the conditional streak sampling outlined above, histograms of streak lift angle statistics for fully-developed near-wall turbulence are shown in Fig. 5 at eduction locations of y^+=10, 20, and 30. Analogous to the definition of θ_{20} above, the streak lift angle at a general y is defined as $\theta_n=\tan^{-1}[|\partial u/\partial z|_{max} / (dU_0/dy)]_{y+=n}$. At y^+=20, comparison of lift angle statistics (Fig. 5b) with the corresponding streak instability growth rate (Fig. 4) indicates that approximately 25% of near-wall streaks are strong enough (*i.e.* with sufficient $\partial u/\partial z$) to be linearly unstable. At y^+=10 and y^+=30 as well, streaks stronger than the neutrally stable analytical streak (of the form (1), indicated by bold line in Fig. 5) occur in fully-developed turbulence. [Thus, not all streaks detected in the buffer layer are strong enough to become unstable.]

In summary, streaks of sufficient strength for linear instability are in fact realized in the buffer layer. Note that at larger y, similar strong streaks are observed, but are much less common (see *e.g.* Robinson 1991). In contrast, most streaks nearer to the wall are numerous, but do not have sufficient lift angles to be linearly unstable and hence are dynamically passive with respect to streak instability. Finally, note that other possible mitigating factors of streak instability, particularly the influence of viscous annihilation of base flow streak vorticity, must also be considered. Additionally, the streak count declines sharply near the stability cutoff (*e.g.* Fig. 5b); while the growth rate increases with increasing streak strength, the number of unstable streaks decreases rapidly (*cf.* Figs. 4, 5b). Hence, a scenario of predominant vortex generation and turbulence sustenance via linear instability of lifted near-wall streaks must be evaluated carefully, as undertaken below.

3.2 Linear transient growth

Having identified linear streak instability of a frozen base flow, we now consider the linear evolution of the instability eigenmode and other x-dependent disturbances of unfrozen, viscously decaying streaks. As shown in Fig. 6 for an initially unstable streak with $\theta_{20}=56°$, the normal mode growth is arrested at $t^+\sim50$ by the streak diffusion, resulting in a factor of two 3D energy growth (i.e. all x-dependent modes). Note that the typical nonlinear (finite amplitude) saturation is not occurring here. Instead, attenuation is due primarily to cross-diffusion (*i.e.* viscous annihilation, a kind of planar reconnection) of the opposite-signed ω_y flanking the low-speed streak. In fact, ω_y is reduced to 70% of its initial value by the E_{3D} saturation time, indicating that the (exponential) streak decay rate due to cross-diffusion is non-negligible (approximately half the instability growth rate).

Significantly, much more significant growth of the arbitrary $w(x)$ perturbation (3) occurs for the same base flow streaks, producing a factor of 20 energy growth (Fig. 6). Recalling the modest factor of two growth of the normal eigenmode, the dominant growth of the $w(x)$ disturbance (3) indicates that its initial rapid amplification is due to *linear transient growth* (see Trefethen *et al.* 1993 for a review of the transient growth concept). In short, transient growth of disturbances is possible for non self-adjoint (*i.e.* non-normal) linearized Navier-Stokes operators, such as derived here for disturbances of two-dimensional streaks. Recall that eigenmodes of traditional normal mode stability problems are not orthogonal to one another if the corresponding linear operator is non-normal. In this case, particular disturbances (including specific combinations of normal eigenmodes) can generally be amplified by significant factors (*i.e.* linear transient growth), even if all normal eigenmodes are individually stable.

In Fig. 6, the early-time evolution of the disturbance (3) is dominated by non-normal mode transient growth (the only means for disturbance growth to exceed that of the most unstable normal mode). Note that the disturbance (3) eventually locks-on to the normal mode and hence excites both the non-normal transient disturbance and the normal eigenmode. Further, the relevance of the disturbance (3) in the actual flow is supported by observations of x-alternating quadrant 2 and 3 uw Reynolds stress events in near-wall turbulence. As further clear evidence of non-normal transient growth, the $w(x)$ disturbance (3) produces a factor of 7 energy growth for linearly stable streaks (*i.e.* no growth due to stable normal eigenmode), growth which is maintained into the nonlinear regime (Fig. 7). Finally, note the distinction of the linear transient growth of streaks $U(y,z)$ revealed here, with the linear transients of the mean profile $U(y)$ studied extensively to date (see *e.g.* Butler & Farrell 1992).

4. Nonlinear evolution and vortex formation

Having confirmed that (one-walled) streaks with sufficient y circulation can experience significant growth of x-dependent disturbances via a combined linear transient/instability mechanism, we now consider the subsequent nonlinear evolution using DNS. Results clearly illustrate the genesis of streamwise CS, near-wall shear layers, and arch vortices, suggesting that streak disturbance growth is the dominant mechanism of vortex generation and thus turbulence production. Most significantly, as the mode grows to a nonlinear amplitude (initially $w'/U_c=1\%$ at $y^+=30$), new collapsed streamwise vortices are directly created (Fig. 8a-c). At early times, disturbance growth is characterized by increased circulation of flattened ω_x sheets, with the spanwise symmetry of the linear eigenmode approximately maintained. Subsequently, as nonlinear effects (described below) become prominent, $+\omega_x$ begins to concentrate on the $+z$ flank of the

low-speed streak (Fig. 8b). By symmetry, the ω_x distribution at a half wavelength in x away is obtained by z reflection and sign inversion; thus, $-\omega_x$ is generated on the $-z$ flank here. As this ω_x amplification continues, collapsed (*i.e.* with compact cross-section) streamwise vortices quickly emerge (Fig. 8c). This genesis of new vortices from ω_x layers is strikingly similar to that frequently observed in minimal channel flow.

Previous studies (*e.g.* Jimenez & Orlandi 1993) have focused on wall vorticity layer rollup due to (2D) self-advection (and image vorticity due to wall impenetrability). In the streak disturbance evolution described here, the vortex formation is not in reality a rollup process; the formation is inherently 3D, dominated by intense ω_x stretching. Even well past their initial formation, streamwise vortices and hence turbulence continue to be sustained (*e.g.* Fig. 8d), indicating the importance of this streak disturbance mechanism to turbulence sustenance.

The 3D geometry of the newly generated vortices (Figs. 9a,b) (say, the x-overlapping of tilted, opposite-signed streamwise vortices on either side of a low-speed streak) agrees well with the typical flow structure during the active phase of minimal channel regeneration. Most significantly, this vortex geometry (maintained upon evolution except for increasing overlap) is strikingly similar to that of 3D CS educed (from more than 100 vortex realizations) in full-domain turbulence (Fig. 10), which has been shown to capture all important near-wall events (Jeong *et al.* 1997). Irregularities (*e.g.* kinks) of the base flow streaks and finite-amplitude incoherent turbulence will surely occur, causing variations in vortices from one realization to another. If an underlying instability mechanism is present, it should be revealed by ensemble averaging over a large number of base flow/perturbation combinations, *i.e.* by CS eduction. The close correspondence of Figs. 9 and 10 indicates that this is in fact the case, serving as strong evidence that this vortex formation process is a dominant mechanism in near-wall turbulence.

Since the newly generated vortices are predominantly streamwise (Fig. 9a), the essential dynamics of vortex formation are those of ω_x, whose inviscid evolution is governed by

$$\frac{\partial \omega_x}{\partial t} = -u\frac{\partial \omega_x}{\partial x} \underbrace{- v\frac{\partial \omega_x}{\partial y} - w\frac{\partial \omega_x}{\partial z}}_{\text{Advection}} + \underbrace{\omega_x \frac{\partial u}{\partial x}}_{\text{Stretching}} + \underbrace{\frac{\partial v}{\partial x}\frac{\partial u}{\partial z} - \frac{\partial w}{\partial x}\frac{\partial u}{\partial y}}_{\text{Tilting}} . \qquad (4)$$

In Fig. 11, we observe that the circulation of the elongated near-wall ω_x layers (Fig. 11a) increases due to vortex line tilting, given by the latter production term $-(\partial w/\partial x)(\partial u/\partial y)$ (Fig. 11c), which dominates the former. Although typically largest in magnitude over all other, the $-(\partial w/\partial x)(\partial u/\partial y)$ term actually generates a flattened tail in the near-wall ω_x layer (C in Fig. 7c), *not* a vortex. Contrary to prior speculation, these layers do not roll up due to their self-advection – a purely 2D mechanism. In fact, the cross-stream transport (B in Fig. 11b) actually opposes the rollup process, due to the opposite-signed ω_x immediately overhead (SN in Fig. 11a). In reality, vortex formation is due to direct stretching of $+\omega_x$ on the $+z$ flank of the low-speed streak (also, $-\omega_x$ amplification on the $-z$ flank, at a half x wavelength away), evident from nearly circular regions of $+\omega_x\partial u/\partial x$ there (D in Fig. 11d). We find that this local ω_x stretching is sustained in time and is mainly responsible for the vortex collapse, whose location coincides with the $+\omega_x\partial u/\partial x$ peak.

In turn, the positive $\partial u/\partial x$ responsible for vortex collapse by stretching is a simple consequence of low-speed streak waviness, illustrated in Fig. 9(a). Recall that streak waviness is generated both by (linear) transient growth and sinuous streak instability.

Once this waviness grows to a finite size, strong $+\partial u/\partial x$ develops downstream of the streak crests, causing direct stretching of positive (SP) and negative (SN) ω_x existing there. Since a large velocity difference exists across the streak flanks (with vorticity comparable to the mean velocity gradient at the wall), a sizable value of $+\partial u/\partial x$ is quickly generated by the rapidly growing streak wave. The initial ω_x sheets (Fig. 8a) then suddenly collapse (Fig. 8c) due to localized stretching (Fig. 11d), overcoming viscous diffusion which would otherwise cause their annihilation (on a similar timescale as the collapse). Note that these dynamics are also captured as (ensemble-averaged) +VISA events (*i.e.* $+\partial u/\partial x$) existing within the CS core (Fig. 10), indicating that this vortex generation process is indeed a dominant one.

5. Concluding remarks

To summarize, we have shown that nonlinearly evolving $w(x)$ disturbances of ejected low-speed streaks, initially without any vortices whatsoever, directly generates new streamwise vortices near the wall. The resulting 3D vortex geometry is identical to that of the dominant CS, educed from fully developed near-wall turbulence, which in turn capture all important, extensively reported near-wall events. This serves as strong evidence that vortex-less streaks are the main breeding ground for new streamwise vortices, commonly accepted as dominant in turbulence production. In turn, the geometry of the newly generated vortices constitutes a built-in mechanism which sustains ejected streaks against their otherwise rapid self-annihilation due to cross-diffusion of ω_y. Vortex-less streaks, the vehicle for vortex formation, are expected to arise inherently due to the differential advection of vortices and the streaks they generate.

Since streamwise vortex formation and the associated enhanced drag appear to be reliant on lifted low-speed streaks with strong ω_y, large-scale (relative to the natural streak spacing) control of streaks is a potentially effective approach to drag reduction. We have demonstrated the feasibility of drag reduction via bulk forcing using either counterrotating vortex generators or colliding spanwise wall jets, requiring no instantaneous flow information (otherwise necessary for adaptive control); see Schoppa & Hussain 1998b for details. For implementation at very high *Re*, the physical scale of our control will likely decrease, but being significantly larger than the near-wall structures, will alleviate the scale limitations of controllers and eliminate the need for sensors.

II. Drag Control Experiments

1. Objective

Recent direct numerical simulations (Schoppa & Hussain 1998, 2000) reveal a new large-scale control scheme for suppressing the generation of drag-enhancing streamwise vortices from streaks. This demonstrates that a significant drag reduction is achievable via a large-scale steady control flow, requiring no sensor, actuator, or instantaneous flow information. The control flow suppresses the streak instability (actually, transient growth of otherwise stable streaks) — responsible for (re)generating drag-enhancing near-wall (buffer-layer) streamwise vortices and thereby significantly reduces drag (and hence turbulent heat transfer).

Our objective was to first demonstrate the drag reduction via proof-of-concept experiments in a small air channel flow facility at low Re_θ values using Large-scale Passive Manipulators (LPM) that generate the control flow of weak counter-rotating streamwise vortices over one wall.

2. Approach

Experiments were performed in an air channel flow facility (45cm long x 49cm wide x 5 cm high) using its bottom (Plexiglas) wall as the test plate. The test plate is allowed to float freely on a liquid bath (figure 12). Note that the length of the test (floating) plate is necessarily kept small so that the flow is a flat plate TBL, not a turbulent channel flow.

The floating plate is set flush with the fixed upstream plate, with the air flow turned off. Turbulence generator (a saw-tooth blade; base width = 4mm and height =1.5mm) is used to trip the boundary layer for it to become fully turbulent (Hussain & Clark 1977). For drag control, we used a spanwise row of 42 LPMs mounted on the flat plate at a downstream distance of 13 cm from the turbulence generator. A single LPM is a half-delta winglet (2mm high and 4mm long) aligned alternately at + α -- the angle of incidence with the flow direction-- such that the LPMs produce alternate clockwise and anti-clockwise largescale streamwise vortices. We varied α over the range + 6 – + 12 degrees and $\alpha = +8^{\circ}$ provided the best result within the velocity range we examined (about 12 m/sec –14 m/sec).

The downstream motion of the floating plate is opposed by a cantilever beam fitted with a strain gauge. Static balance of forces on the plate is thus achieved, and the strain gauge measures the net drag (including form and skin-friction drag due to the LPMs) on the plate. Since there is no motion in the liquid bath, all drag experienced by the plate is due to the air flow. The strain gauge can measure force with a resolution of 0.5 milligram, which corresponds to the measurement of a change in drag to within 0.03% even at a fairly low free-stream velocity (say 3m/s). The accuracy is expected to be higher at higher air velocities.

3. Progress

Originally, we started measuring drag on the plate by hanging the test plate with two long strings. For a given velocity, the hanging plate deflected downstream by the drag, and the plate was forced back to its original position using counterweights. To keep the plate vertical under flow condition, we had to arrest the plate's transverse motion using bearings. Because of poor measurement resolution and bearing friction, we developed the floating plate measurement technique. This technique has one problem; at speeds higher than about 25m/sec the plate becomes unstable and force measurement is not possible. At lower speeds, the streamwise motion of the test plate is smooth and stable.

We are currently considering a new system to improve further the drag measurement resolution by an order of magnitude and at a much higher Re values (see section 5) .

4. Results

For drag control (as discussed in section 2) we used 42 (21 pairs) of LPMs such that each alternate winglets are oppositely inclined (yawed) to the streamwise direction and generate swirls of opposite signs. The near-wall control flow is thus like alternating spanwise wall-jets superimposed on the TBL. The z-separation of wall-jet collision (streamwise) lines, being much larger than the average streak spacing (z^+=100), enables control of many streaks by each control flow vortex (swirl). The streaks are squeezed

together in one-half of a swirl and spread apart in the other half. Both effects cause weakening of the streaks, making their flank slope fall below the instability limit: cross-diffusion or planar reconnection in the first case and flattening (or swatting) of streaks in the second case.

In our experiments, LPM height roughly equals four times the displacement thickness (δ^* about 0.5mm in the velocity range of 12 m/s to 25m/sec), and their spanwise spacing is chosen to be a few times the streak spacing

With the current measurement system using one strain gauge (which is not temperature compensated compared to 2 or 4 strain gauge system) the net drag reduction shows some
variation from experiment to experiment which is about 4% to 11%. This variation is perhaps because of temperature variation and angular setting of the LPMs.

Figure 13 shows one set of our results indicating noticeable drag reduction. For example, drag reduction are about 11%, 11.5% and 8% for U= 15.25, 18.25, and 24.5 m/sec respectively.

5. Future Plan

(a) Currently, we are considering a few options to measure TBL drag directly using: (i) full bridge-strain gauge system (i.e. four strain gauges: two in tension and two in compression) which are temperature compensated and have high resolution. (ii) Differential Variable Reluctance Transducer (DVRT) which can measure displacement with a resolution of 10 nanometer. This system will require properly calibrated springs – low spring constant for low velocities and high spring constant for high velocities to utilize the full stroke length of the DVRT.

(b) Use miniature step motors to set LPM angles accurately via remote control without disturbing the test plate. Alternate LPMs can be connected to a worm grear driven by a single motor so that inclination angles of these alternate LPMs can be changed simultaneously and identically. Another worm gear will connect the other set of the alternate LPMs.

(c) Once the drag reduction is conclusively established with a single spanwise row of LPMs, we will systematically vary for a single Re_θ the LPM parameters, viz. the angle of attack of the half-delta winglets (which affects the circulation and streamwise extent of the swirling control flow, as well as device drag), their spanwise spacing (which determines the number of streaks influenced by a single LPM), and their height (which is expected to crucially influence both device drag penalty and the transverse location of the center of the control flow swirl). The height of the LPMs will be selected from the measured local displacement thickness (*). We will use two LPM heights, viz. 8 * and 4 *, i.e. close to the boundary layer thickness and half of that. Two transverse spacing of LPMs will be used, viz 25 and 50 streak spacing. These spacing will be estimated from the measured wall units.

(d) To measure drag as well as shear stress, experiments will be performed in a low-noise in-house (1m wide x 1.6m high x 7m long test section) wind tunnel. A carefully designed and machined floating plate setup similar to the one used in the channel flow facility will be built

(e) This tunnel will facilitate hot-wire measurements within the sublayer. The estimated sublayer thickness near the end of the tunnel is about 0.25mm and hot-wire measurements will provide about 8 data points within the sublayer, allowing an accurate estimate of the wall shear stress (τ_w) employing Clauser cross plot method.

(f) Hot-wire measurements will be performed at three transverse location viz. at the middle location of a pair of LPMs and near the trailing edge of the LPMs. For each transverse location, boundary layer characteristics (viz. the mean and turbulence quantities, τ_w) will be measured at a few streamwise location These data will indicate the drag reducing effect of the first row of LPMs and will dictate the placement of the next row of LPMs. Direct drag measurements will be carried out with two rows of LPMs over a range of Re_θ (3000-8000) to delineate the range of effectiveness of this scheme.

(g) Develop code for prediction for flow around LPMs and for drag reduction.

(h) Educe CS structures in LPM wake using a cross-wire rake, compare with numerical predictions and improve code.

(i) Study feasibility for heat transfer control by measuring local heat transfer behind LPMs with heated air/wall.

(j) Study the feasibility of applying LPM in aircraft for drag reduction.

References

Butler, K.M. & Farrell, B.F. 1992 Three-dimensional optimal perturbations in viscous shear flow. *Phys Fluids A* **4**, 1637.

Hamilton, J., Kim, J. & Waleffe, F. 1995 Regeneration mechanisms of near-wall turbulence structures. *J. Fluid Mech.* **287**, 317.

Hussain, A.K.M.F. & Clark, A. R. 1978 Upstream Influence on the Near Field of a Plane Turbulent Jet. *Phys. Fluids* **20**, 1416.

Hussain, F. 1986 Coherent structures and turbulence. *J. Fluid Mech.* **173**, 303.

Jeong, J. & Hussain, F. 1992 Coherent structures near the wall in a turbulent channel flow. In *Proc. of Fifth Asian Congress of Fluid Mech.*, Taejon, Korea (eds. K.S. Chang & H. Choi), p. 1262.

Jeong, J. & Hussain, F. 1995 On the identification of a vortex. *J. Fluid Mech.* **285**, 69

Jeong, J., Hussain, F., Schoppa, W. & Kim, J. 1997 Coherent structures near the wall in a turbulent channel flow. *J. Fluid Mech.* **332**, 185.

Jimenez, J. & Moin, P. 1991 The minimal flow unit in near-wall turbulence. *J. Fluid Mech.* **225**, 213.

Jimenez, J. & Orlandi, P. 1993 The rollup of a vortex layer near a wall. *J. Fluid Mech.* **248**, 297.

Kim, J., Moin, P. & Moser, R.D. 1987 Turbulence statistics in fully developed channel flow at low Reynolds number. *J. Fluid Mech.* **177**, 133.

Kline, S.J., Reynolds, W.C., Schraub, F.A. & Rundstadler, P.W. 1967 The structure of turbulent boundary layers. *J. Fluid Mech.* **30**, 741.

Robinson, S.K. 1991 Coherent motions in the turbulent boundary layer. *Ann. Rev. Fluid Mech.* **23**, 601.

Schoppa, W., Hussain, F. & Metcalfe, R.W. 1995 A new mechanism of small-scale transition in a plane mixing layer: core dynamics of spanwise vortices. *J. Fluid. Mech.* **298**, 23.

Schoppa, W. & Hussain, F. 1997 Genesis and dynamics of coherent structures in near-wall turbulence. In *Self-sustaining Mechanisms of Wall Turbulence* (ed. R. Panton). Computational Mechanics Publications, p. 385.

Schoppa, W. & Hussain, F. 1998a Formation of near-wall streamwise vortices by streak instability. *AIAA Paper* No. AIAA 98-3000.

Schoppa, W. & Hussain, F. 1998b A large-scale control strategy for drag reduction in turbulent boundary layers. *Phys. Fluids* **10**, 1049.

Schoppa, W. & Hussain, F. 2000 Coherent structure dynamics in near-wall turbulence. *Fluid Dyn. Res.* **26**, 119.

Swearingen, J.D. & Blackwelder, R.F. 1987 The growth and breakdown of streamwise vortices in the presence of a wall. *J. Fluid Mech.* **182**, 225.

Trefethen, L.N., Trefethen, A.E., Reddy, S.C. & Driscoll, T.A. 1993 Hydrodynamic stability without eigenvalues. *Science* **261**, 578.

Yu, X. & Liu, J.T.C. 1991 On the secondary instability in Gortler flow. *Phys. Fluids A* **3**, 1845.

Figure 1. Lifted low-speed streaks (black) illustrated by u'<0 at y^+=20 and streamwise vortices (grey) indicated by the Jeong & Hussain (1995) vortex definition in the region 0<y^+<60.

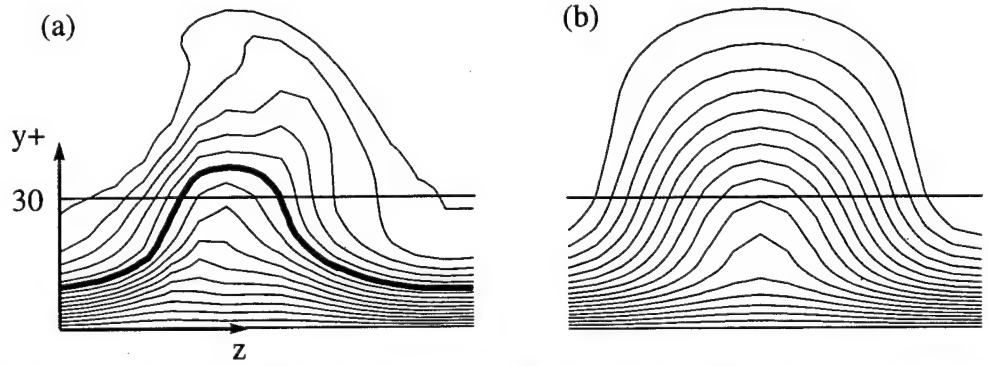

Figure 2. Lifted low-speed streak in near-wall turbulence, illustrated by (a) a typical cross-stream distribution of U, approximated by (b) the analytical base flow (1) used for stability analysis. The bold contour shown in (a) is the $0.55U_c$ contour.

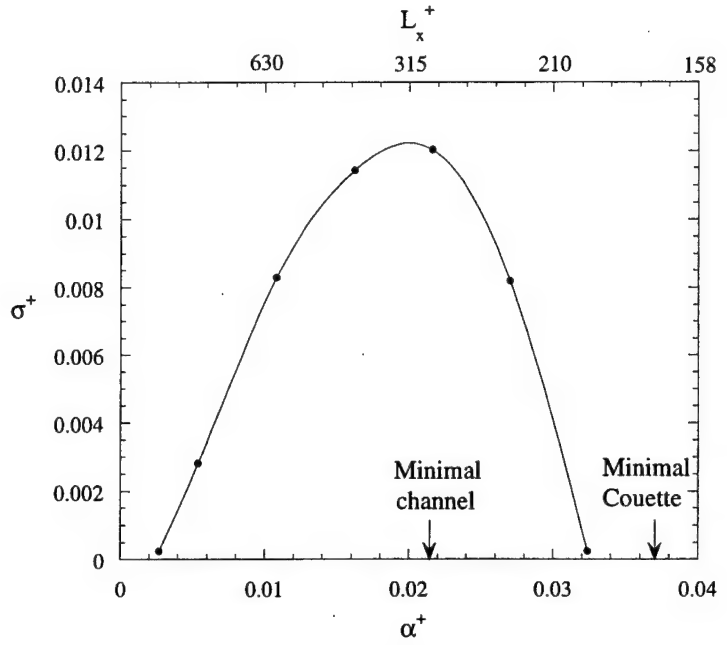

Figure 3. Growth rate of most-unstable sinuous mode versus streamwise wavenumber, for streak distribution in figure 1 with $\omega_y^+|_{max}=0.35$, corresponding to a streak lift angle of $\theta_{20}=56°$.

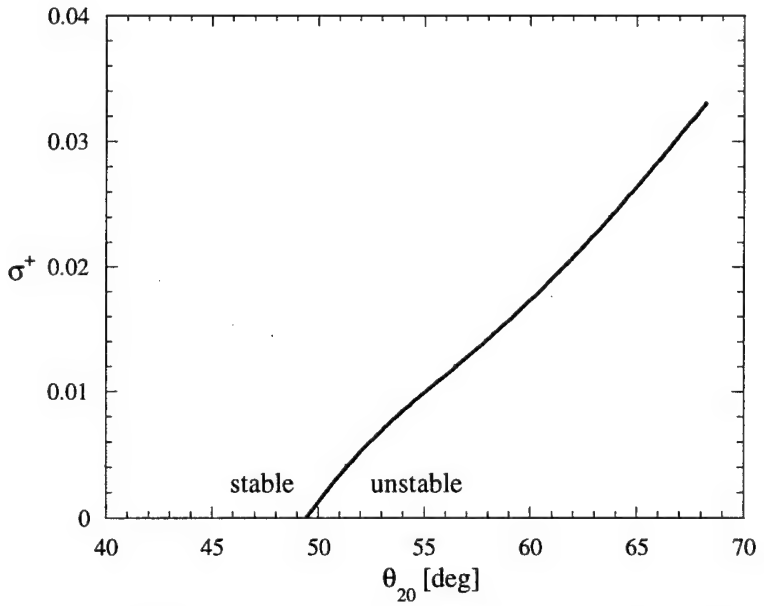

Figure 4. Dependence of sinuous mode growth rate on streak vortex line angle θ_{20} at Re=2000, illustrating threshold of streak lifting required for streak instability growth.

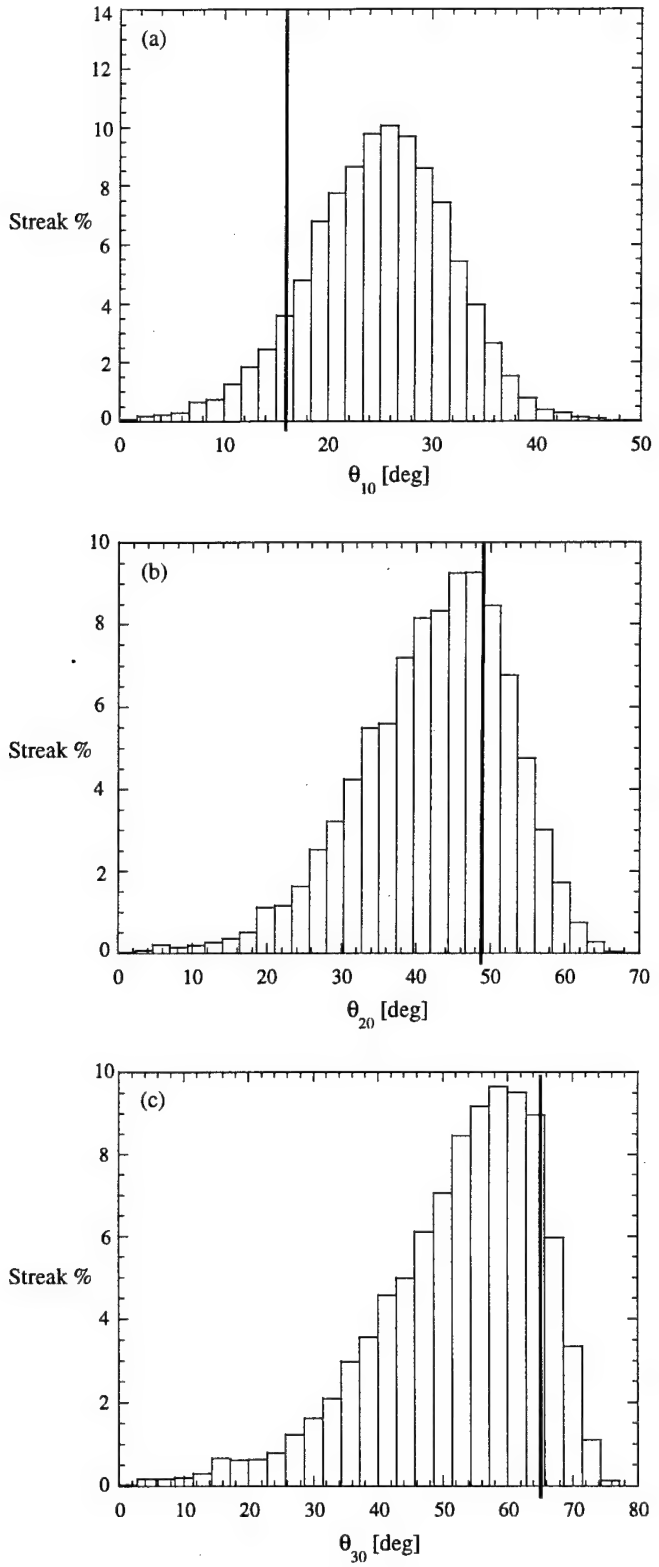

Figure 5. Histograms of conditional streak vorticity statistics, for streaks educed at (a) $y^+=10$, (b) $y^+=20$, and (c) $y^+=30$ from fully developed channel flow turbulence. The bold line in each denotes the instability cutoff in Fig. 4.

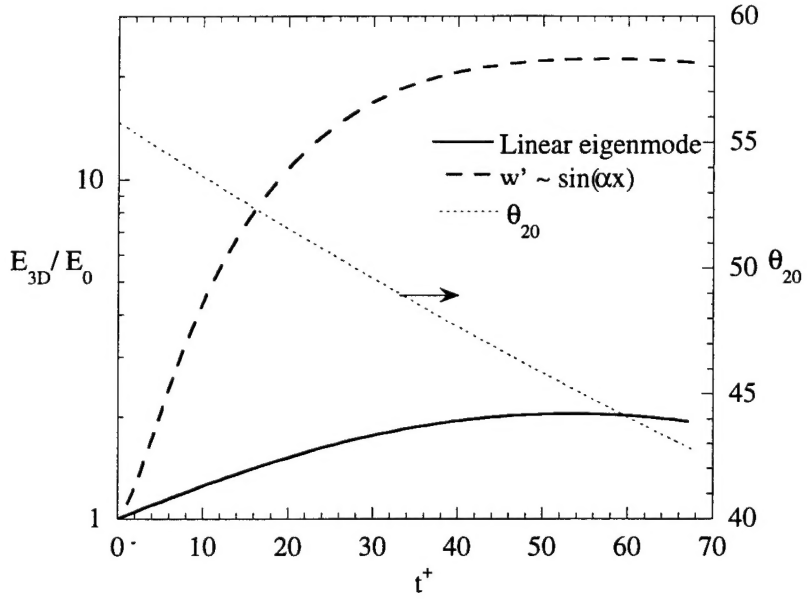

Figure 6. Evolution of 3D energy (all x-dependent modes), for most unstable linear eigenmode (solid) and $w(x)$ linear transient distrubance (dashed). The viscous streak annihilation is reflected by the decreasing streak vortex line lift angle (dotted).

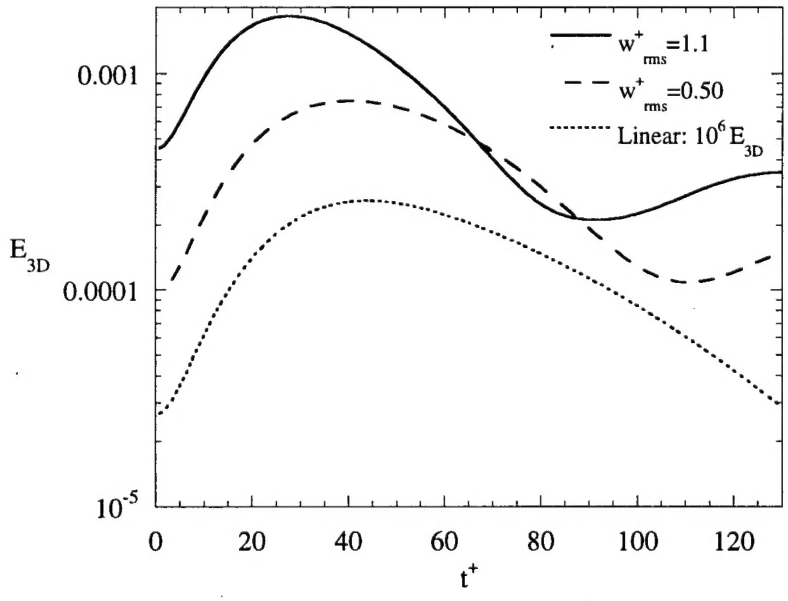

Figure 7. Evolution of 3D energy for w(x) transient disturbance of a linearly stable streak with θ_{20}=45°, for both linear (dotted) and finite-amplitude initial disturbance amplitudes.

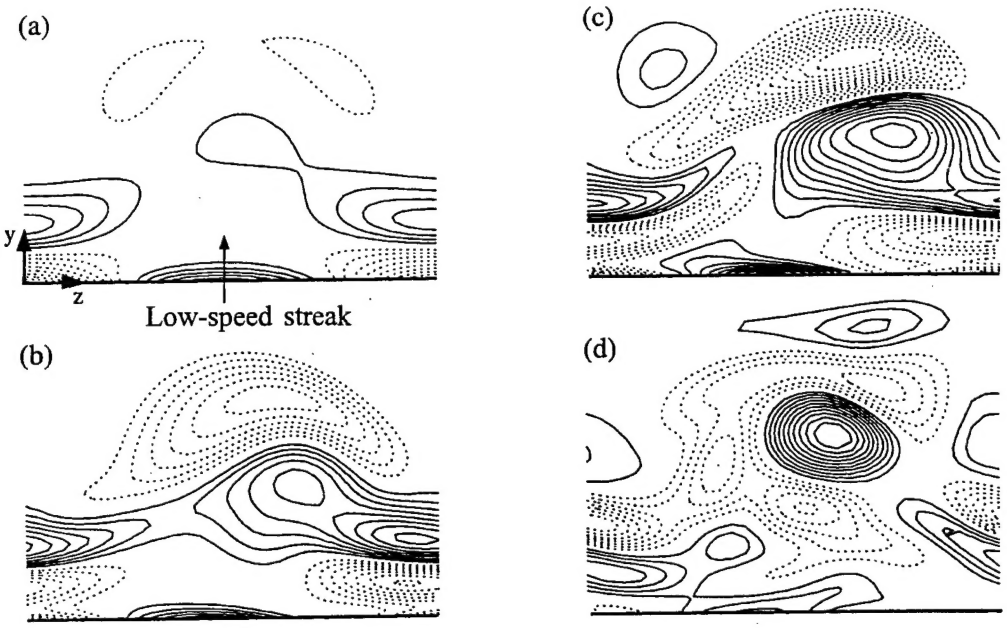

Figure 8. Streamwise vortex formation due to finite-amplitude streak instability, illustrated by cross-stream distributions of ω_x at (a) t^+=17, (b) t^+=51, (c) t^+=103, (d) t^+=928. Planes in (b) and (c) are tracked with the instability phase speed of approximately $0.6U_c$.

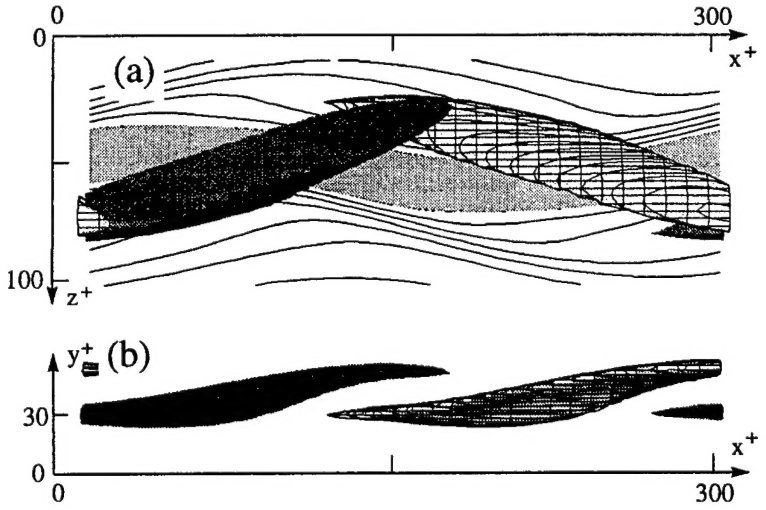

Figure 9. Streamwise vortices' (x,z) plane tilting, x-overlapping, and location relative to a low-speed streak in (a) top view, (b) side view. The 80% isosurfaces of $+\omega_x$ and $-\omega_x$ at t^+=103 are (dark) shaded and hatched respectively; contours of u at y^+=20 are overlaid in (a), with low levels of u light-shaded to demarcate the low-speed streak.

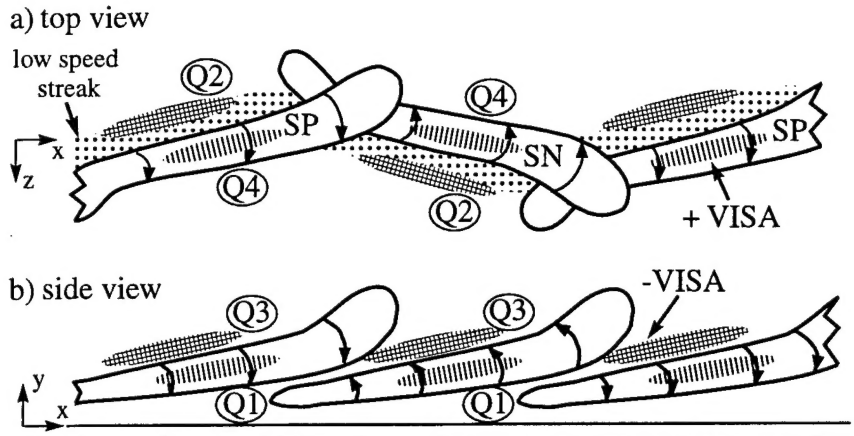

Figure 10. Near-wall educed CS and associated coherent events (adapted from Jeong *et al.* 1997); including ±VISA events ($\pm\partial u/\partial x$); quadrant *Re* stresses Q1, Q2 (ejection), Q3, and Q4 (sweep); and a kinked low-speed streak.

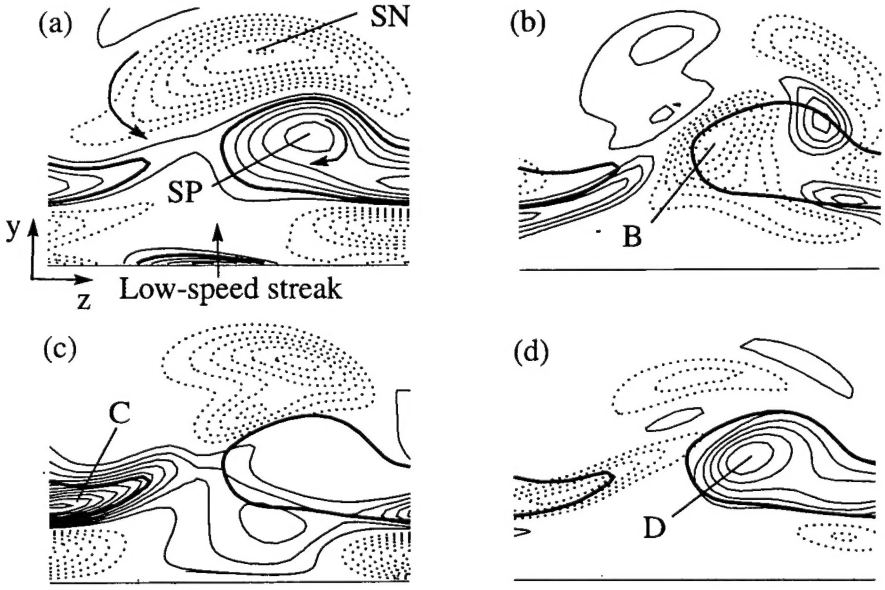

Figure 11. Distributions of (a) ω_x, and selected terms of the ω_x evolution equation: (b) self-induction (cross-stream), (c) the $-(\partial w/\partial x)(\partial u/\partial y)$ tilting term, and (d) direct stretching $(\omega_x \partial u/\partial x)$; (a-d) are at an intermediate time during vortex formation (t^+=51). The bold line in each panel identifies the ω_x layer.

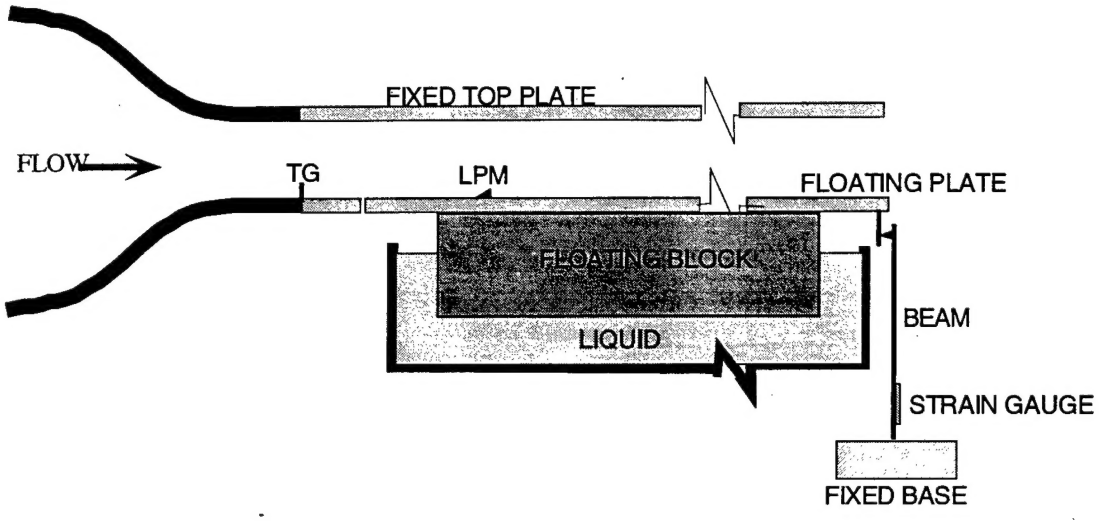

Figure 12. Schematic showing the side cross-sectional view of the channel flow facility. TG: Turbulence Generators; LPM: Large-scale Passive Manipulators.

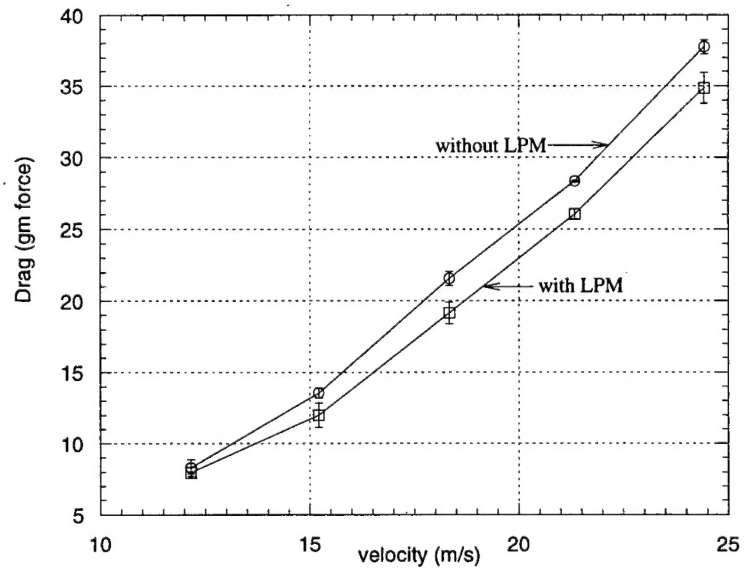

Figure 13. Total drag on the floating plate without and with LPM control.